Journal of Applied Electrochemistry (2026) 56:135
https://doi.org/10.1007/s10800-026-02521-3

RESEARCH ARTICLE

Green synthesis of lead oxide nanostructures using *Passiflora edulis* peel extract and investigation of their electrochemical response toward ethanol oxidation

Ruan Santos da Cruz[1] · Andreza Miranda Barata da Silva[2] · Elizomar Medeiros Barbosa[3] · Noelle Carneiro de Figueiredo[3] · Jocely de Lucena Dutra[3] · João Pedro Ribeiro Barrile[2] · José Wilmo da Cruz Júnior[4] · Elson Almeida de Souza[3] · Thiago Henrique Döring[4] · Eduardo Guilherme Cividini Neiva[5] · Paulo José Sousa Maia[1,2]

Received: 7 December 2025 / Accepted: 9 May 2026 / Published online: 5 June 2026
© The Author(s) 2026

Abstract

An aqueous *Passiflora edulis* peel extract was used to prepare lead oxide nanostructures, which were then tested as modifiers of carbon paste electrodes for ethanol oxidation in acidic medium. Structural, thermal, and morphological features were examined by ultraviolet-visible spectroscopy, X-ray diffraction, Fourier transform infrared spectroscopy, thermogravimetric analysis, scanning electron microscopy coupled to energy-dispersive X-ray spectroscopy, and transmission electron microscopy. The synthesized material consisted of a Pb_3O_4-rich mixed lead oxide system with lamellar morphology and surface-associated phytochemical residues. Among the tested compositions, the electrode containing 5 wt% oxide combined the highest apparent electroactive area with the favorable voltammetric response. The ethanol-oxidation response depended strongly on electrolyte acidity and reached its highest value in 0.5 mol L^{-1} sulfuric acid ($pH \approx 0.3$). Scan-rate analysis suggested a mixed response with an important diffusion contribution and interfacial surface effects. Chronoamperometry and continuous cycling showed that the modified electrode retained electrochemical activity over the test period, whereas impedance measurements at open-circuit potential were consistent with a comparatively low interfacial charge-transfer barrier.These results indicated that *Passiflora edulis* peel extract can be used as a biomass-derived reagent for the preparation of lead oxide nanostructures for ethanol oxidation studies.

✉ Paulo José Sousa Maia
paulomaia@ufscar.br

[1] Federal University of Rio de Janeiro, Macaé, RJ, Brazil

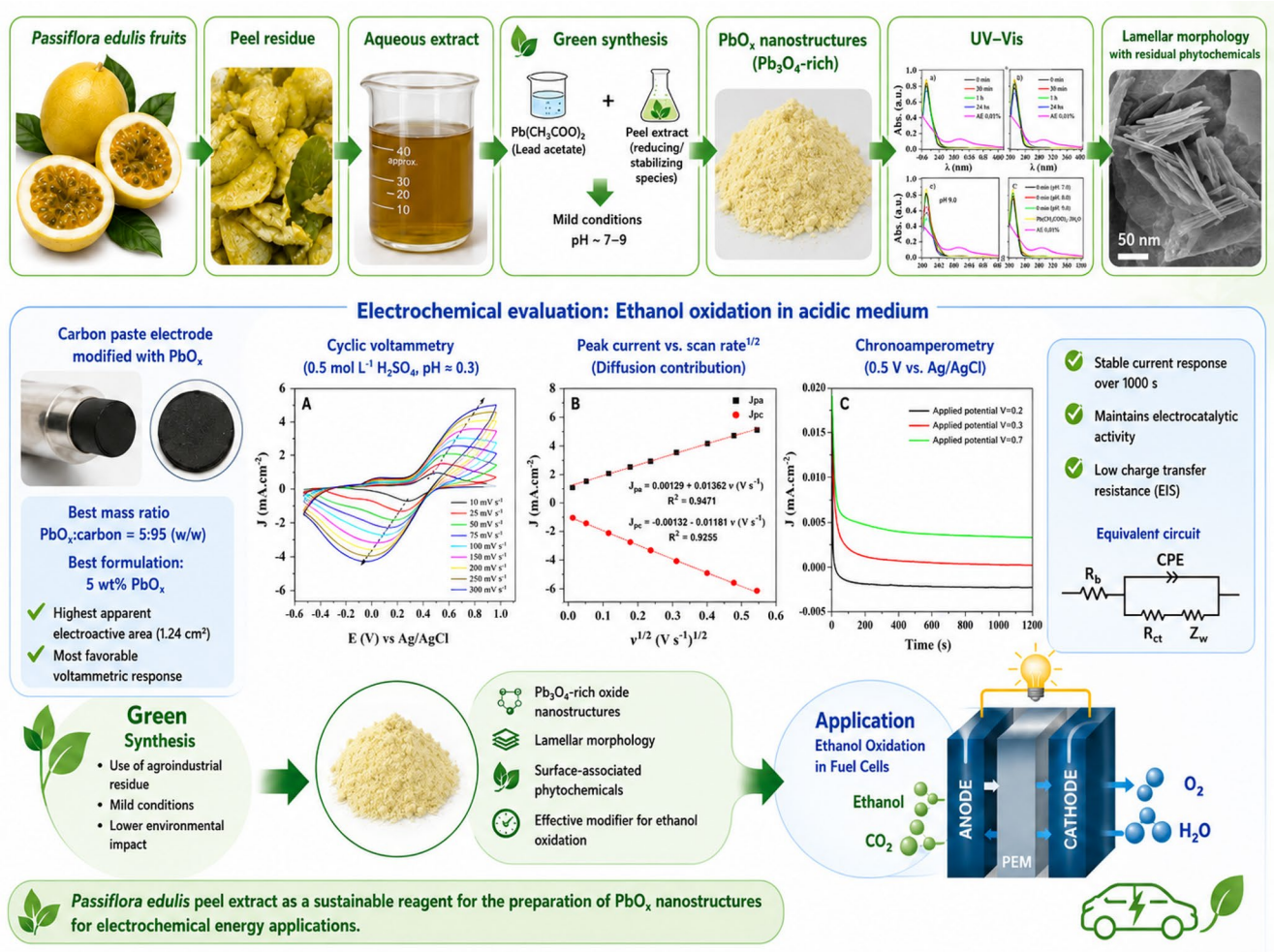
[2] Federal University of São Carlos, Sorocaba, SP, Brazil

[3] Federal University of Amazonas, Itacoatiara, AM, Brazil

[4] Universidade Federal de Santa Catarina, Blumenau, SC, Brazil

[5] Universidade Regional de Blumenau, Blumenau, SC, Brazil

Graphical-Abstract



Keywords Green synthesis · Carbon paste electrode · Acidic medium · Lead oxide nanostructures · Electrochemical response

1 Introduction

Plant-mediated synthesis has become an useful route for preparing nanomaterials because plant extracts can provide reducing, complexing and stabilizing species under relatively mild conditions. This strategy can reduce the harsher reagentes and also allows agricultural residues to be incorporated into the synthetic process [1–3].

Among such residues, *Passiflora edulis* peel is a promising raw material because it is abundant and contains phenolic compounds, flavonoids, and other oxygenated biomolecules that may influence both nanostructure formation and surface stabilization [4, 5]. This residue also offers a straightforward waste-to-material route because it couples waste valorization with the preparation of functional materials.

Pb-based systems, however, require careful consideration. Although plant-mediated routes can make the preparation step less severe, they do not eliminate the toxicological concerns associated with lead-containing materials. Accordingly, the interest in such systems lies in controlling composition, morphology, and interfacial properties rather than in presenting them as intrinsically safe materials [6, 7].

Lead oxide nanostructures have been studied because of their electronic properties and their possible use in sensing, photocatalysis, energy-related devices, and electrochemical systems [8–10]. Ethanol oxidation is especially relevant in this scenario because of its connection with direct ethanol fuel cells and the continuing search for lower-cost catalytic materials. Although Pt- and Pd-based catalysts still dominate this field, their cost and limited availability continue to motivate the study of alternative compositions and surface

modifiers [2, 11]. In this regard, Pb-containing oxides have previously been associated with changes in the adsorption behavior of poisoning intermediates and with enhanced alcohol oxidation response in specific electrode architectures [12].

In the present study, aqueous *Passiflora edulis* peel extract was used to prepare lead oxide nanostructures, and the resulting material was tested as a modifier of carbon paste electrodes for ethanol oxidation in acidic medium. The study focused on how composition, morphology, and interfacial behavior were related in this Pb_3O_4-rich system.

2 Materials and methods

2.1 Materials

Lead(II) acetate trihydrate [$Pb(CH_3COO)_2{\cdot}3\ H_2O$] was obtained from Sigma-Aldrich. Ethanol, sulfuric acid, sodium hydroxide, and mineral oil were used as received. Graphite powder with a specific surface area of 240 $m^2\ g^{-1}$ was used as the carbon matrix for electrode preparation. All aqueous solutions were prepared with deionized water. Yellow passion fruit peels (*Passiflora edulis* Sims f. *flavicarpa*) were collected from local markets in Macaé, RJ, Brazil (22°22′18″S, 41°47′9″W). Unless otherwise stated, electrochemical experiments were performed at 25 °C, and the electrolyte solutions were deaerated with nitrogen for 15 min before analysis.

2.2 Preparation of *Passiflora edulis* peel extract and synthesis of lead oxide nanostructures

Dried and powdered *P. edulis* peels (1.0 g) were mixed with 100 mL of distilled water and heated at 70 °C for 1 h under magnetic stirring. The resulting extract was filtered through Whatman No. 1 filter paper and stored at 4 °C until use.

For nanoparticle synthesis, 5 mL of the aqueous peel extract was added to 500 mL of a 1.0 mmol L^{-1} aqueous $Pb(CH_3COO)_2{\cdot}3H_2O$ solution. The mixture was maintained under stirring at 50 °C for 24 h. The resulting solid phase was allowed to settle, separated, and dried at 90 °C for 4 h. To evaluate the influence of pH on nanoparticle formation, the reaction medium was adjusted to pH 7.0, 8.0, and 9.0 using NaOH solution before the synthesis step.

2.3 Electrode preparation

Carbon paste electrodes (CPEs) were prepared by thoroughly mixing 60 mg of graphite powder with 40 µL of mineral oil in a quartz mortar until a homogeneous paste was obtained. Modified electrodes were prepared by incorporating the lead oxide nanostructures into the carbon paste at 5, 10, and 15 wt%. These three loadings were selected as an exploratory range representing low, intermediate, and relatively high oxide contents while preserving the conductivity and mechanical integrity of the carbon paste matrix. The resulting pastes were packed into a glass tube (3.32 mm internal diameter; 2.2 mm depth), and electrical contact was established with a platinum wire.

2.4 Physicochemical characterization

UV–Vis spectra were recorded on a Shimadzu UV-1800 spectrophotometer using quartz cuvettes (1.0 cm optical path). Samples were dispersed at 0.1 g L^{-1} in 1% HCl (v/v). X-ray diffraction (XRD) measurements were carried out on a Shimadzu XRD-6000 diffractometer using CuKα radiation (λ = 1.5418 Å), operating at 40 kV and 30 mA. Fourier transform infrared (FTIR) spectra were obtained on a Bruker spectrometer equipped with an ATR accessory, using a resolution of 4 cm^{-1} and 20 scans. Thermogravimetric analysis (TGA) was performed on a PerkinElmer TGA-4000 in synthetic air from 50 to 850 °C at a heating rate of 10 °C min^{-1}.

Scanning electron microscopy (SEM) images were acquired on a Tescan microscope operated at 10 kV, and elemental composition was assessed by energy-dispersive X-ray spectroscopy (EDS) using an Oxford detector. Transmission electron microscopy (TEM) images were obtained on a JEOL instrument operated at 120 kV in bright-field and dark-field modes. For TEM analysis, samples were dispersed in deionized water, drop-cast onto carbon-coated copper grids, and dried at room temperature.

2.5 Electrochemical measurements

Electrochemical measurements were performed using an Autolab potentiostat/galvanostat in a conventional three-electrode cell containing the unmodified or modified carbon paste electrode as the working electrode, a platinum disk counter electrode (2 mm diameter), and an Ag/AgCl (3 mol L^{-1} KCl) reference electrode. All potentials are reported versus Ag/AgCl.

The apparent electroactive area of the electrodes was estimated from cyclic voltammetry using the Randles-Sevcik relationship and a 1.0 × 10^{-3} mol L^{-1} hexacyanoferrate redox probe in 0.5 mol L^{-1} K_2SO_4 recorded at different scan rates (Fig. S1). The apparent electroactive areas estimated for the electrodes were 0.184 cm^2 for the bare CPE, 1.24 cm^2 for CPE-PbOx 5%, 0.986 cm^2 for CPE-PbOx 10%, and 0.930 cm^2 for CPE-PbOx 15%. In porous carbon paste systems, the value obtained from the Randles-Sevcik equation should be interpreted as a comparative apparent electroactive area rather than as a true geometric area, because surface

roughness, porosity, and heterogeneous accessibility of the redox probe contribute to the calculated value [13–16].

The effect of electrolyte acidity on the electrochemical response of CPE–PbOx 5% was evaluated by cyclic voltammetry in solutions with pH values of 0.3, 1.0, 3.0, 5.0, and 7.0. The strongly acidic condition corresponded to 0.5 mol L−1 H2SO4 (pH≈0.3). The effect of ethanol concentration was subsequently investigated in the 0.2–1.0 mol L^{-1} range under the selected acidic condition. Scan-rate studies were performed between 0.01 and 0.30 V s^{-1}. Chronoamperometric measurements were carried out to evaluate the time-dependent current response and short-term operational stability.

Electrochemical impedance spectroscopy (EIS) measurements were performed using an Autolab PGSTAT 128 N system in a Faraday cage over the frequency range from 104 to 10^{-2} Hz, using an AC amplitude of 10 mV and the open-circuit potential in the presence of 1.0 mol L^{-1} ethanol at pH 0.3. Nyquist and Bode representations were used for data analysis.

3 Results and discussion

3.1 Formation and physicochemical characterization of the lead oxide nanostructures

The UV-Vis spectra recorded for the materials synthesized at pH 7.0, 8.0, and 9.0 exhibited a main absorption band centered at 208 nm (Fig. 1), which is consistent with electronic transitions associated with oxidized Pb species. The absence of a broad band in the visible range argues against the formation of metallic Pb-rich colloids and is more compatible with oxide-dominated lead nanostructures.

Lead-based oxide nanostructures generally do not present the intense localized surface plasmon resonance typical of noble-metal nanoparticles because their electronic structure and free-electron density are substantially different. Thus, the high-energy absorption observed in Fig. 1 is consistent with oxidized lead phases and with charge-transfer transitions involving Pb-O bonds and surface-coordinated organic species.

The XRD pattern (Fig. 2A) indicated that the synthesized material was predominantly composed of tetragonal Pb_3O_4 (ICDD PDF 01–085-0859), whereas weaker reflections at approximately 25.4°, 32.0°, 36.2°, and 49.1° were consistent with PbO_2 (ICDD PDF 01–078-0313), suggesting the presence of a secondary oxide phase. These results indicate that the plant-mediated synthesis yielded a mixed lead oxide material rather than a single chemically uniform phase [17–20].

Additional evidence for the hybrid inorganic/organic nature of the material was obtained from FTIR and TGA. The FTIR spectrum (Fig. S2) showed bands at 3466 cm^{-1} (νO–H), 2928 cm^{-1} (νC–H), 1757 cm^{-1} (νC = O), 1151/1105 cm^{-1} (νC–O–C), and 1058/1022 cm^{-1} (νC–O), indicating that organic constituents from the extract remained associated with the oxide surface after synthesis and drying. Bands

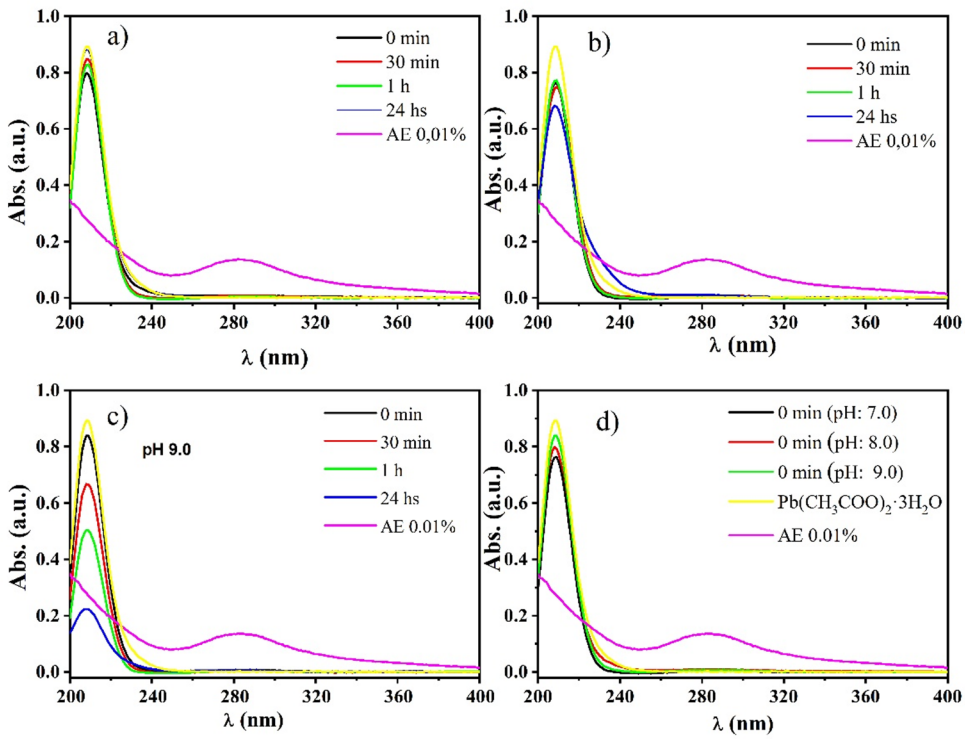


Fig. 1 UV–Vis spectra of the dispersions obtained from the synthesis of lead oxide nanostructures using aqueous *P. edulis* peel extract under different initial pH conditions. **a** pH 7.0, **b** pH 8.0, and **c** pH 9.0. Spectra were recorded immediately after sample preparation at 25 °C. **d** Comparative UV–Vis spectra of the lead acetate precursor solution, the aqueous *P. edulis* peel extract (AE 0.01%), and the dispersions obtained after synthesis at pH 7.0, 8.0, and 9.0

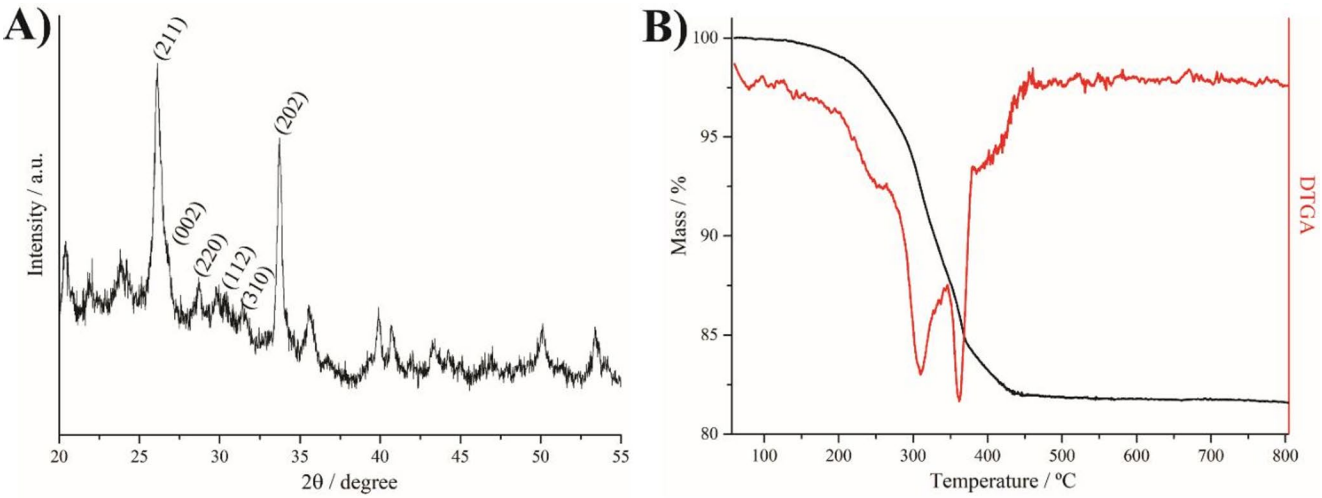


Fig. 2 **A** XRD pattern of the lead oxide nanostructures synthesized using aqueous *P. edulis* peel extract. **B** TGA and DTGA curves of the synthesized material recorded in synthetic air after pre-treatment at 100 °C for 20 min, showing thermal events at 254, 309, 362, and 402 °C and a total mass loss of 18.1%

in the low-wavenumber region, at 537 and 465 cm^{-1}, were consistent with Pb–O vibrations, reinforcing the assignment of lead oxide phases [21, 22].

The TGA and DTGA curves (Fig. 2B) revealed a multistep thermal degradation process between 200 and 450 °C, with thermal events centered at 254, 309, 362, and 402 °C, resulting in a total mass loss of 18.1%. The mass-loss are compatible with decomposition of organic material associated with the extract and possibly with residual acetate-derived species from the precursor [23–25].

SEM images (Fig. 3A–C) revealed flower-like agglomerates formed by overlapping lamellar subunits. These structures consisted of thin plates with average thicknesses of approximately 30 nm, assembled into secondary agglomerates with diameters in the 1–2 µm range, as estimated from the micrographs using ImageJ. The EDS spectrum (Fig. 3D) confirmed Pb and O as the dominant inorganic elements, while C and Na were attributed to residual plant-derived species and reaction by-products. TEM analysis (Fig. 3E) further resolved plate-like domains at the nanoscale and showed an individual nanosheet with an approximate lateral dimension of 380 nm.

These results indicate that the material is composed of thin oxide lamellae aggregated into larger hierarchical secondary structures, which supports the use of the term nanostructures rather than a simplified description as isolated spherical nanoparticles. Although the microscopy data clearly support a lamellar architecture, the absence of a full particle-size distribution analysis using ImageJ or equivalent image-processing treatment limits a more rigorous assessment of morphological uniformity and dispersion.

Although the microscopy data clearly support a lamellar morphology, the absence of particle-size distribution analysis prevents a more rigorous quantitative morphological discussion. Even so, the combined SEM and TEM observations are sufficient to establish a multiscale architecture composed of thin oxide plates assembled into micrometric agglomerates.

3.2 Selection of the modified electrode based on apparent electroactive area

Among the tested formulations, the carbon paste electrode containing 5 wt% Pb-based oxide displayed the highest apparent electroactive area (1.24 cm^2), followed by lower values for the bare CPE and for the electrodes containing 10 and 15 wt% modifier. Thus, due the most pronounced voltammetric response, the 5 wt% composition was selected for further electrochemical evaluation. The voltammograms in Fig. S1 suggest that this loading offers a more favorable compromise between the presence of electroactive PbOx species and the maintenance of the conductive graphite network. Increasing the oxide content beyond this level did not improve the response; instead, the lower apparent electroactive areas at 10 and 15 wt% may reflect less efficient electron percolation and a less favorable electrode microstructure.

3.3 pH-dependent electrochemical response in the supporting electrolyte

The pH-dependent voltammetric response of CPE-PbOx 5% in the supporting electrolyte is shown in Fig. S3, with the direct comparison at 10 mV s^{-1} presented in Fig. S3F. The current response was highest at pH 0.3 and progressively decreased as the pH increased toward neutral conditions. In strongly acidic medium, the Pb-based surface

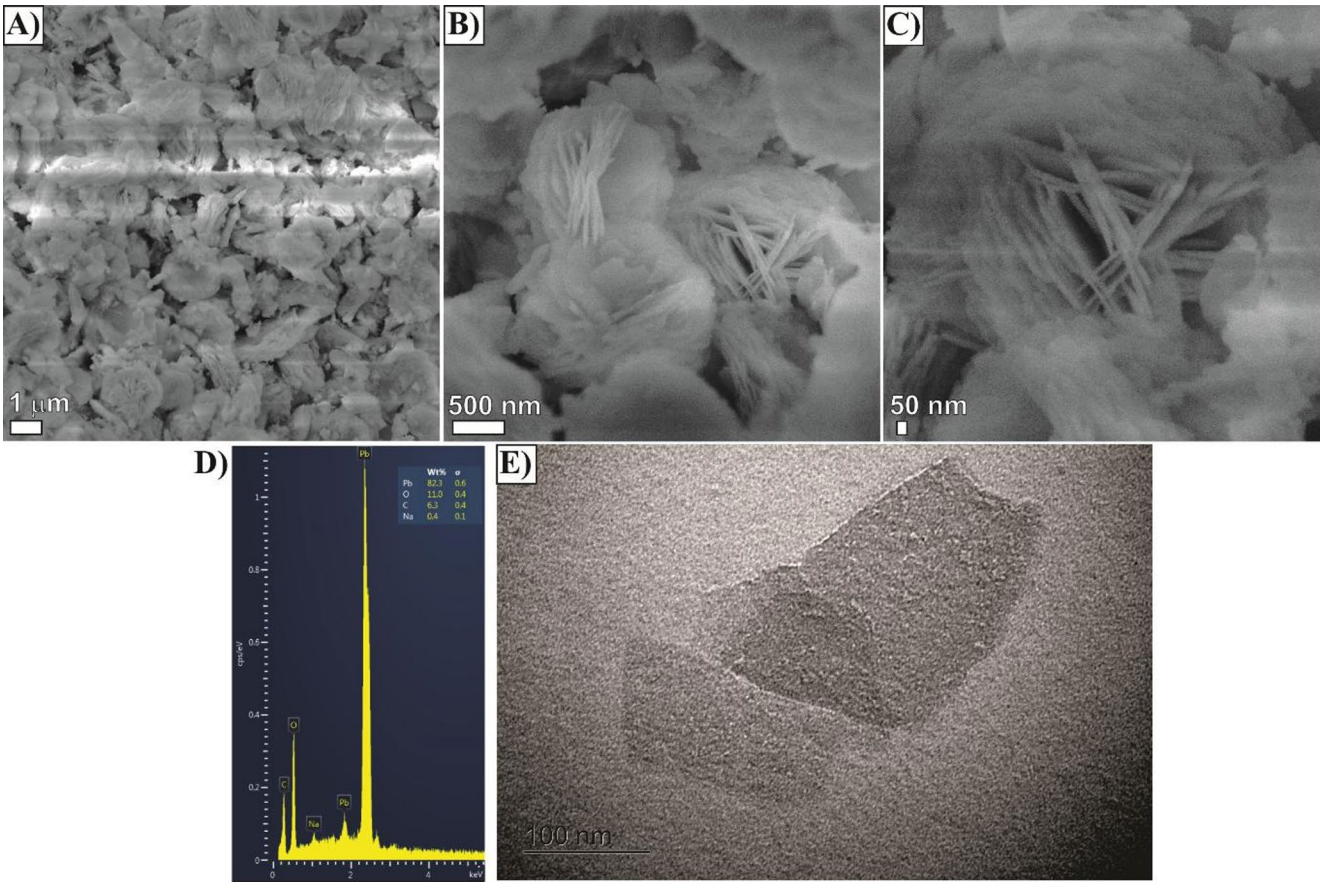


Fig. 3 **A**–**C** SEM micrographs, **D** EDS spectrum, and **E** TEM image of the PbOx nanostructures synthesized using *P. edulis* peel extract

species appear to undergo better-defined redox transitions, whereas at higher pH values the voltammetric features become broader and less intense. This behavior is consistent with the strong influence of proton activity on the interfacial chemistry of lead oxides in sulfuric acid media and supports the use of pH 0.3 as the most favorable condition for the subsequent ethanol-oxidation experiments [26].

3.4 Scan-rate dependence in the supporting electrolyte

The electrochemical behavior of CPE-PbOx 5% in the supporting electrolyte was further examined as a function of scan rate (Fig. S4). As shown in Fig. S4A, both anodic and cathodic peak current densities increased with increasing scan rate, indicating acceleration of the redox response under faster potential perturbation. The current-scan-rate relationships shown in Fig. S4B and Fig. S4C indicate that the system cannot be described by a purely idealized single-control model.

For the anodic curve, current varied more linearly with scan rate than with the square root of scan rate, indicating a significant surface contribution to the response. The cathodic branch, however, showed poorer linearity in both representations, suggesting the coexistence of charge-transfer, surface reorganization, and mass-transport effects. The increase in ΔEp with scan rate (Fig. S4D), clearly exceeding the value expected for a reversible one-electron process, further indicates quasi-reversible to irreversible behavior. These results show that, even in the absence of ethanol, the PbOx-modified electrode exhibited a non-ideal redox response that serves as a baseline for the interpretation of the voltammetric behavior in alcohol-containing medium [13].

3.5 Electrochemical response toward ethanol oxidation

3.5.1 Effect of electrolyte acidity

The voltammetric response of CPE-PbOx 5% in the absence and presence of ethanol at different pH values is shown in Fig. 4. The highest anodic and cathodic current densities in the presence of ethanol were observed at pH 0.3, indicating that strongly acidic medium favored the electrochemical response of ethanol on the modified electrode. As the

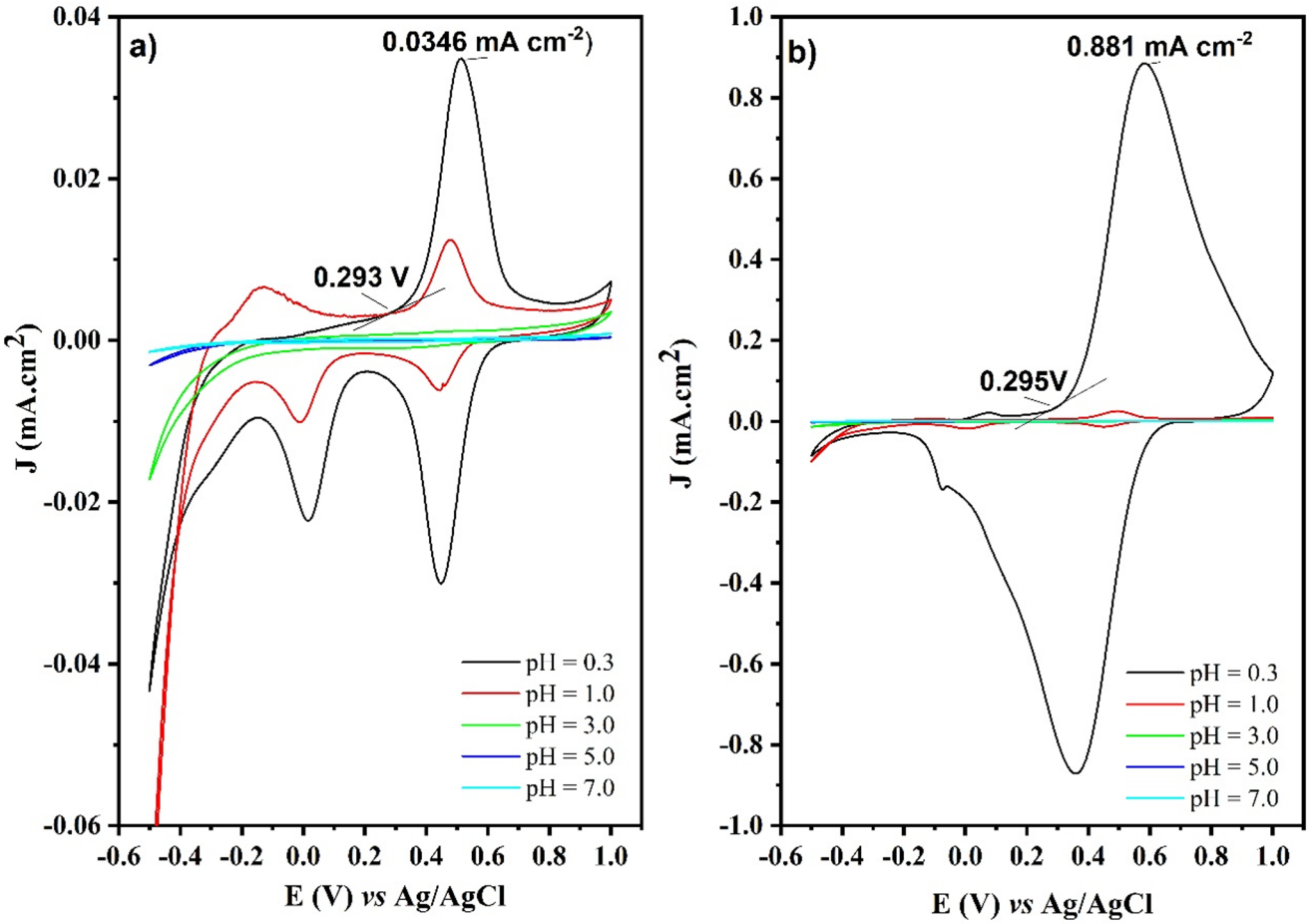


Fig. 4 Cyclic voltammograms of CPE-PbOx 5% recorded at different pH values in the **a** absence and **b** presence of 1.0 mol L^{-1} ethanol. Scan rate: 10 mV s^{-1}. Temperature: 25 °C. Apparent electroactive area: 1.24 cm^2

pH increased, the current density decreased progressively, showing that the electrode response is strongly dependent on proton availability.

The higher response in acidic medium is consistent with faster proton-coupled surface steps and with more rapid turnover of oxygenated Pb-containing surface species. At higher pH, the voltammetric response became weaker and broader, which suggests slower interfacial turnover and less efficient removal of adsorbed partially oxidized species. Thus, the pH profile in Fig. 4 is consistent with the baseline behavior already observed in Fig. S3 and confirms pH 0.3 as the most suitable condition for the subsequent mechanistic and stability analyses [12–28]. Although the strongly acidic medium maximized the voltammetric response, partial dissolution of Pb-containing surface species under these conditions cannot be excluded and should be addressed in future stability and leaching studies.

3.5.2 Effect of scan rate on ethanol oxidation

The effect of scan rate on the ethanol oxidation response of CPE-PbOx 5% at pH 0.3 is shown in Fig. 5.

Both anodic and cathodic peak currents increased as the scan rate increased, which is consistent with a faster voltammetric response under more rapid potential sweeps. The best linearity was obtained when peak current was plotted against the square root of scan rate (Fig. 5c), indicating that diffusion of ethanol and other solution-phase species toward the electrode surface contributed significantly to the observed response.

At the same time, the direct current-versus-scan-rate plots also showed substantial linearity (Jpa, $R^2 = 0.9952$; Jpc, $R^2 = 0.9181$), which means that the process should not be described as exclusively diffusion-controlled. The data are better described by mixed control, with a significant diffusional contribution superimposed on interfacial effects related to adsorption and surface reorganization.

The increase in peak separation with scan rate (Fig. 5d) indicates progressively more irreversible behavior at higher

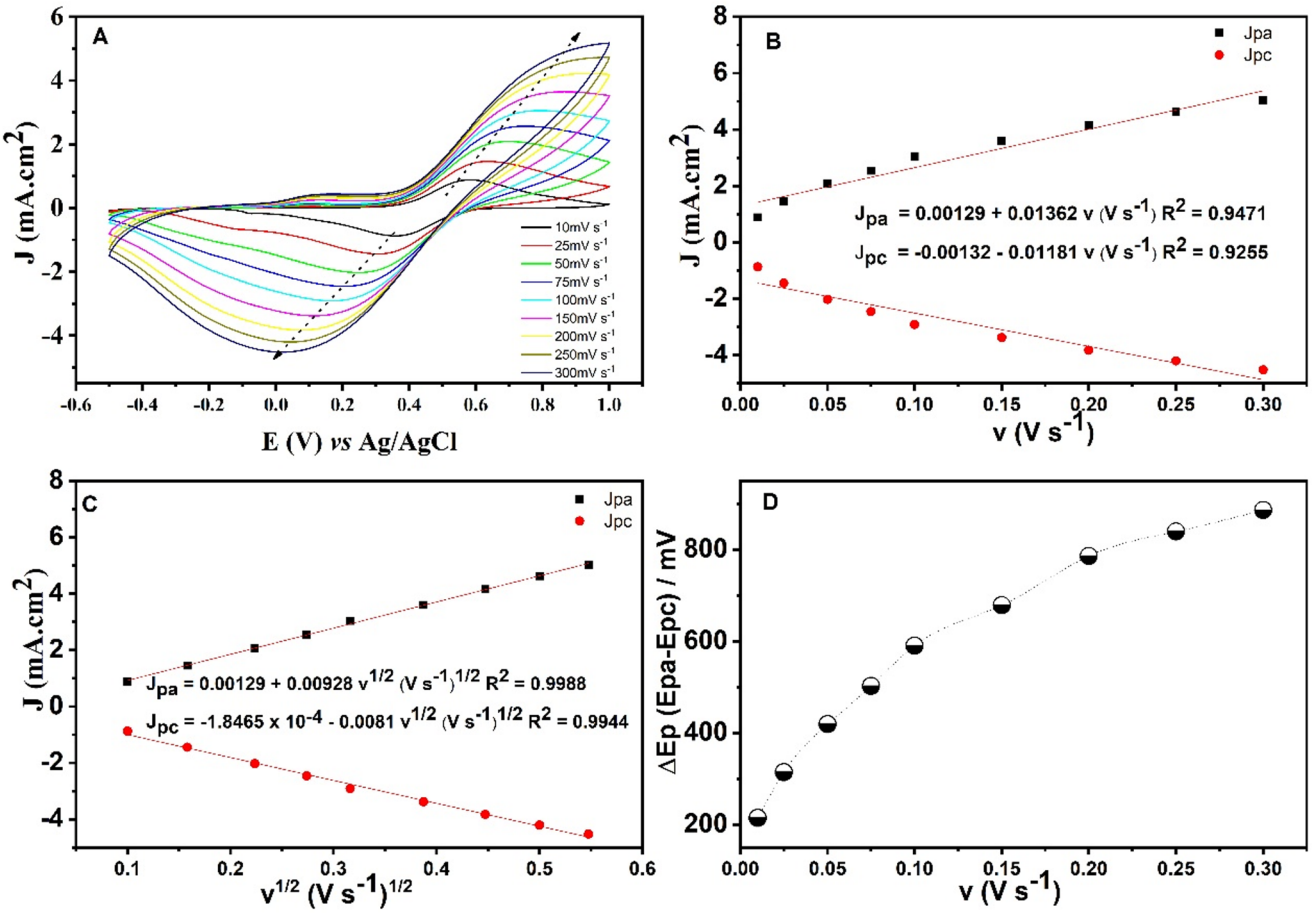


Fig. 5 **a** Cyclic voltammograms of CPE-PbOx 5% in 1.0 mol L^{-1} ethanol at pH 0.3 recorded at different scan rates (0.01–0.30 V s^{-1}). **b** Peak current density versus scan rate. **c** Peak current density versus the square root of scan rate. **d** Peak-to-peak separation (ΔEp) *versus* scan rate. Temperature: 25 °C. Apparent electroactive area: 1.24 cm^2

scan rates, which is compatible with slower charge-transfer kinetics and with the growing influence of adsorbed intermediates on the interfacial response. Accordingly, the voltammetric data support a diffusion-dominated but not diffusion-exclusive mechanism under the investigated conditions [13, 29],

Similar scan rate-dependent broadening of ΔEp has been reported for non-noble-metal electrocatalysts based on Fe, Cu, and Ni-containing systems, in which incomplete regeneration of active surface sites under fast potential sweeps contributes to non-ideal voltammetric behavior [30, 31].

3.5.3 Effect of ethanol concentration

Figure 6 shows that increasing ethanol concentration from 0.1 to 1.0 mol L^{-1} led to a systematic increase in anodic peak current density. The linear relationship between anodic current and ethanol concentration (Fig. 6b) indicates that, within the investigated concentration range, the response increased proportionally with substrate availability and that no obvious saturation of active sites was reached.

This result shows that the modified electrode remains responsive within the concentration window investigated and that the electrochemical response can be tuned by ethanol concentration under strongly acidic conditions. Nevertheless, this linearity alone does not establish pseudo-first-order kinetics, because voltammetric current responses under the present conditions do not isolate reaction order.

What the data do support is a concentration-dependent enhancement of current without clear evidence of site saturation in the studied range. This behavior is consistent with an interface that still offers available PbOx-related active domains as the ethanol concentration increases, while mass transport from the bulk solution remains sufficiently fast to sustain the response.

The absence of major shifts in peak potential suggests that increasing ethanol concentration primarily changes the magnitude of the response rather than the voltammetric profile. In practical terms, this is favorable because it indicates

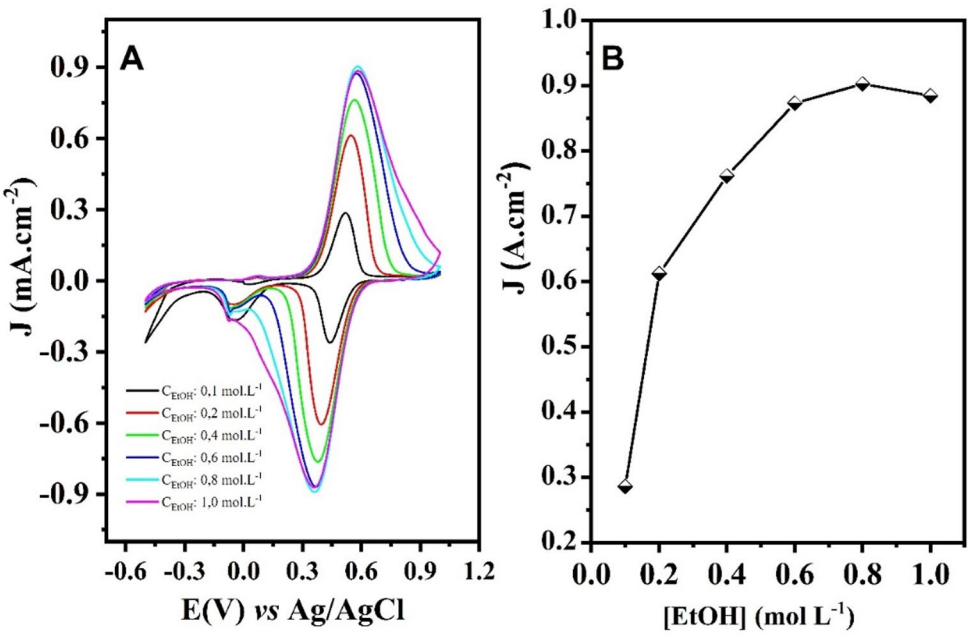


Fig. 6 **a** Cyclic voltammograms of CPE-PbOx 5% in 0.5 mol L^{-1} H_2SO_4 containing increasing ethanol concentrations (0.1–1.0 mol L^{-1}) at pH 0.3. **b** Linear correlation between anodic peak current density and ethanol concentration. Scan rate: 10 mV s^{-1}. Temperature: 25 °C. Apparent electroactive area: 1.24 cm^2

that the modified electrode retains its characteristic response over a concentration range relevant to ethanol-electrooxidation studies.

Fig. 6 indicates that ethanol concentration modulates the current response of CPE-PbOx 5% in a predictable manner, reinforcing the suitability of the selected acidic condition for comparative electrochemical investigation.

3.5.4 Chronoamperometric response and cycling stability

Chronoamperometric measurements and continuous cyclic voltammetry were used to evaluate the time-dependent response and short-term electrochemical stability of the modified electrode in 1.0 mol L^{-1} ethanol at pH 0.3 (Fig. 7). Chronoamperometric responses were recorded at fixed potentials of 0.2, 0.3, and 0.7 V vs. Ag/AgCl 3 M.

At 0.2 V, the measured currents were low, which is consistent with operation below the region of more intense ethanol oxidation response and with a limited faradaic contribution. The corresponding current densities were − 0.000895 mA cm^{-2} for the bare CPE and − 0.00364 mA cm^{-2} for CPE–PbOx 5%. By contrast, at 0.3 and 0.7 V the current decayed rapidly in the initial stage and then evolved toward a more stable response, as shown in Fig. 7A and B. This behavior is commonly associated with double-layer charging, rapid local consumption of ethanol near the electrode surface, and the transient accumulation of adsorbed partially oxidized species, followed by slower replenishment of reactants from the bulk solution [27, 29, 32].

Compared with the unmodified CPE, the PbOx-modified electrode showed higher current values, indicating that the incorporated oxide material contributes to the ethanol-oxidation response. In the cycling experiment, the increase in peak current density over 50 scans suggests progressive surface activation or conditioning rather than immediate deactivation. A possible interpretation is therefore that the electrode remained electrochemically active over repeated scans and may have undergone beneficial surface rearrangement during cycling, although this evidence alone is not sufficient to demonstrate long-term operational durability.

After approximately 200 s, the bare CPE approached a near steady-state current, whereas CPE–PbOx 5% stabilized only after about 500–600 s. The longer transient observed for the modified electrode may reflect its larger accessible interfacial area, slower establishment of adsorbate coverage, and continued activation of available PbOx-related surface domains as ethanol diffuses and reacts at the interface.

To further evaluate electrochemical robustness, continuous cyclic voltammetry was performed for 50 consecutive cycles from −0.5 to 1.1 V for 50 cycles (Fig. 7C, D). The increase in peak current density over scans suggests progressive surface activation or conditioning rather than immediate deactivation. A cautious interpretation is that the modified electrode remained electrochemically active during repeated cycling and may have undergone beneficial surface rearrangement, such as partial removal of passivating species or gradual exposure of additional active domains. Nevertheless, these results should be interpreted as evidence of short-term electrochemical stability only, since 50 cycles are not sufficient to demonstrate long-term operational durability under device-relevant conditions.

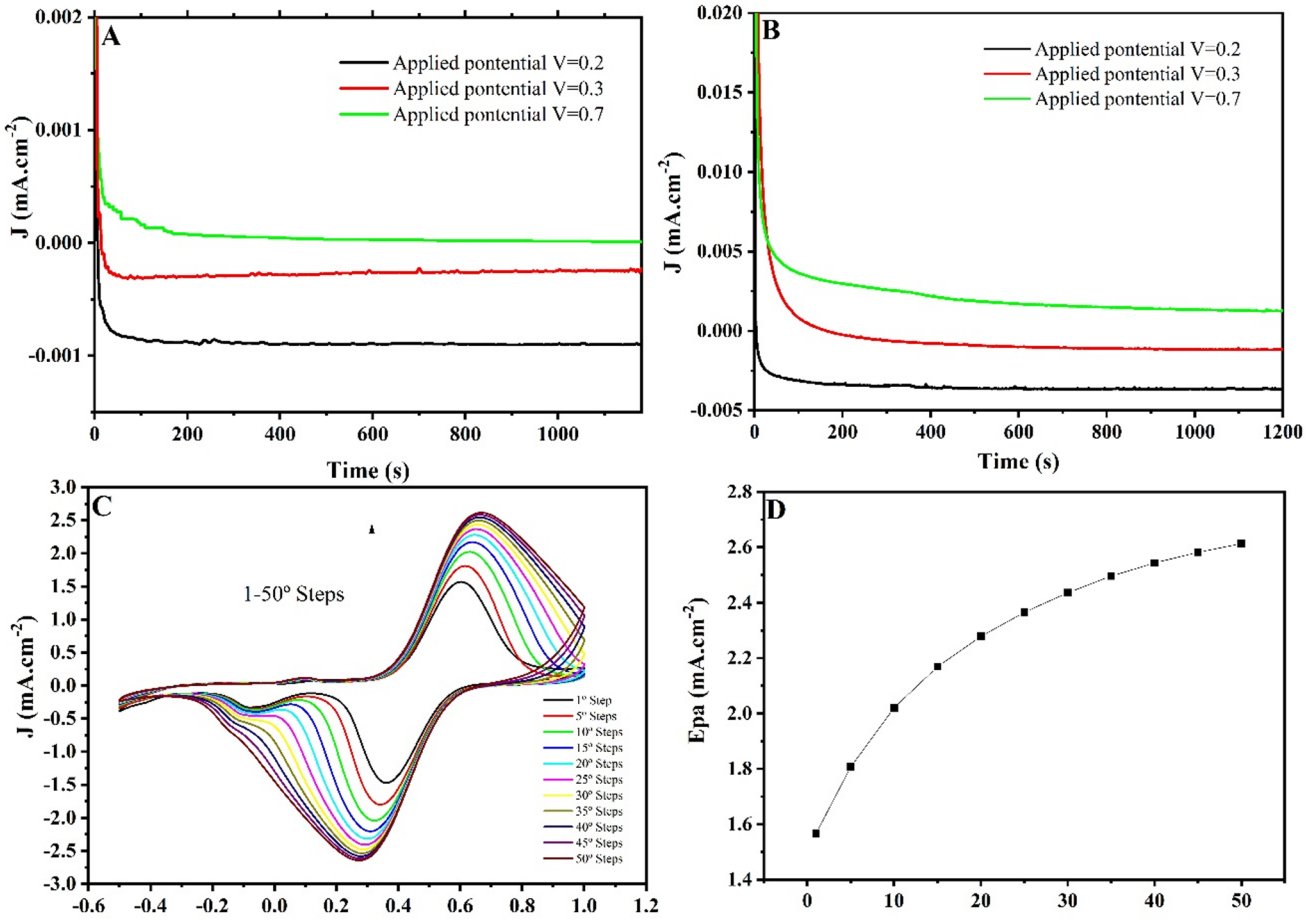


Fig. 7 **A** Chronoamperometric responses of the bare CPE and **B** CPE-PbOx 5% recorded at 0.2, 0.3, and 0.7 V in 0.5 mol L^{-1} H_2SO_4 containing 1.0 mol L^{-1} ethanol at pH 0.3. **C** Continuous cyclic voltammetry over 50 cycles and **D** evolution of peak current density during cycling. Temperature: 25 °C. Apparent electroactive area: 1.24 cm^2

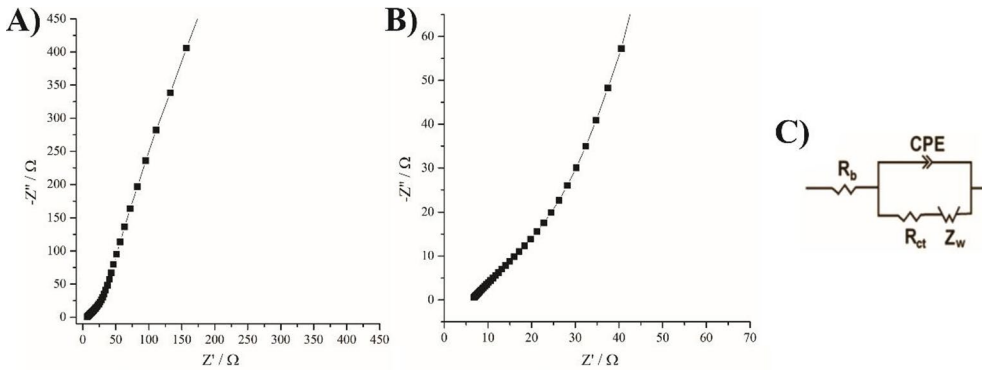


Fig. 8 **A**, **B** Electrochemical impedance spectra of CPE-PbOx 5% recorded in 1.0 mol L^{-1} ethanol at pH 0.3 and open-circuit potential. **C** Equivalent circuit used for fitting the impedance data

3.6 Electrochemical impedance spectroscopy

Electrochemical impedance spectroscopy was used to evaluate the interfacial properties of CPE-PbOx 5% in ethanol-containing acidic medium at pH 0.3 and open-circuit potential (Fig. 8).

The Nyquist plot displayed a high-frequency semicircle followed by a lower-frequency diffusional contribution, consistent with the coexistence of charge-transfer and mass-transport effects at the electrode/electrolyte interface. The Bode representation complements this interpretation by showing a frequency-dependent response characteristic of a non-ideal interfacial process rather than that of a simple purely resistive system.

The comparatively small semicircle diameter suggests a relatively facile interfacial charge-transfer process under the

measured condition, whereas the low-frequency tail indicates the contribution of diffusional transport. Because the measurement was performed at open-circuit potential, the impedance results should be interpreted as describing the interfacial state of the system in ethanol-containing acidic medium rather than the reaction kinetics at the anodic oxidation peak.

Using the equivalent circuit shown in Fig. 8C, the spectrum was fitted in terms of a combined bulk/contact resistance (Rb), a constant phase element (CPE), a charge-transfer resistance (Rct), and a Warburg-type diffusional element (Zw). The fitted Rct value of 35 Ω is consistent with the relatively small high-frequency semicircle and indicates that the PbOx-modified interface does not impose a severe kinetic barrier under the measured interfacial state. This interpretation is also coherent with the mixed charge-transfer/diffusion regime inferred from cyclic voltammetry, although the impedance result should not be overinterpreted as a direct kinetic descriptor at the oxidation-peak potential.

4 Conclusion

This study demonstrated that Passiflora edulis peel extract can be used as a biomass-derived reagent in the synthesis of lead oxide nanostructures through a plant-mediated route. The obtained material was predominantly composed of tetragonal Pb3O4 and exhibited a lamellar morphology, with spectroscopic and thermal evidence indicating the presence of residual organic species associated with the nanostructure surface.

Among the tested electrode formulations, the carbon paste electrode containing 5 wt% PbOx showed the largest apparent electroactive area and the most favorable voltammetric response toward ethanol oxidation. The electrochemical behavior was strongly influenced by the acidity of the medium, and the best response was observed at pH 0.3. Scan-rate analysis suggested that ethanol oxidation occurs under a diffusion-dominated but not diffusion-exclusive regime, whereas chronoamperometry and cycling experiments indicated that the modified electrode remained electrochemically active during repeated measurements.

, the results support the use of Passiflora edulis peel extract as a suitable precursor medium for the preparation of Pb-based oxide nanostructures and indicate that the resulting material is a relevant candidate for further studies on ethanol electrooxidation. Future work should focus on improving compositional control, evaluating long-term operational stability, and clarifying the reaction mechanism and interfacial charge-transfer behavior under the optimal catalytic conditions. Despite the use of a plant-mediated synthetic route, any practical application of Pb-based oxide materials will require careful assessment of lead leaching, operational stability, and end-of-life management.

Supplementary Information The online version contains supplementary material available at https://doi.org/10.1007/s10800-026-02521-3.

Acknowledgements This study was supported by Fundação Carlos Chagas Filho de Amparo à Pesquisa do Estado do Rio de Janeiro (FAPERJ; E-26/210.070/2022, SEI-260003/015957/2021, SEI-260003/015018/2021-APQ1, and E-26/201.248/2022-SEI-260003/003411/2022-BBP), Fundação de Amparo à Pesquisa do Estado de São Paulo (2025/09305-6), CAPES (Coordenação de Aperfeiçoamento de Pessoal de Nível Superior; Finance Code 001), and CNPq (Conselho Nacional de Desenvolvimento Científico e Tecnológico). The authors also thank PPGCM-UFSCar (Programa de Pós-Graduação em Ciência dos Materiais), PPGCTRA-UFAM (Programa de Pós-Graduação em Ciência e Tecnologia para Recursos Amazônicos), Professor Dr. Aldo José Gorgatti Zarbin and GQM-UFPR for the XRD and SEM analyses, and CLAIMS-FURB for the FTIR and TGA analyses.

Author contributions Ruan Santos da Cruz, Andreza Miranda Barata da Silva, Elizomar Medeiros Barbosa, Noelle Carneiro de Figueiredo, Jocely de Lucena Dutra, João Pedro Ribeiro Barrile, José Wilmo da Cruz Júnior, Elson Almeida de Souza, Thiago Henrique Döring, and Eduardo Guilherme Cividini Neiva contributed to material preparation, data collection, and data analysis. Paulo José Sousa Maia supervised the study and contributed to the study conception and design. All authors contributed to manuscript writing, critical revision, and approval of the final version.

Funding The Article Processing Charge (APC) for the publication of this research was funded by the Coordenação de Aperfeiçoamento de Pessoal de Nível Superior - Brasil (CAPES) (ROR identifier: 00x0ma614).

Data availability No datasets were generated or analysed during the current study.

Declarations

Competing interests The authors declare no competing interests.

Open Access This article is licensed under a Creative Commons Attribution 4.0 International License, which permits use, sharing, adaptation, distribution and reproduction in any medium or format, as long as you give appropriate credit to the original author(s) and the source, provide a link to the Creative Commons licence, and indicate if changes were made. The images or other third party material in this article are included in the article's Creative Commons licence, unless indicated otherwise in a credit line to the material. If material is not included in the article's Creative Commons licence and your intended use is not permitted by statutory regulation or exceeds the permitted use, you will need to obtain permission directly from the copyright holder. To view a copy of this licence, visit http://creativecommons.org/licenses/by/4.0/.

References

1. Iravani S, Zolfaghari B (2013) Green synthesis of silver nanoparticles using *Pinus eldarica* bark extract. Biomed Res Int. https://doi.org/10.1155/2013/639725
2. Cruz JF, dos Santos Batista J, da Silva AMB, da Silva EM, Laier LO, Dutra JL, da Cruz JW Júnior, Perotti GF, Cividini Neiva EG, de Souza EA, Sousa Maia PJ (2025) Exploring the electrochemical properties of platinum nanoparticles synthesized by green synthesis using *Paullinia cupana* extract. Mater Sci Eng B Adv Funct Mater. https://doi.org/10.1016/j.mseb.2025.118632
3. Kharissova OV, Dias HVR, Kharisov BI, Pérez BO, Pérez VMJ (2013) The greener synthesis of nanoparticles. Trends Biotechnol 31:240–248. https://doi.org/10.1016/j.tibtech.2013.01.003
4. Ramli ANM, Manap NWA, Bhuyar P, Azelee NIW (2020) Passion fruit (Passiflora edulis) peel powder extract and its application towards antibacterial and antioxidant activity on the preserved meat products. SN Appl Sci 2:1748. https://doi.org/10.1007/s42452-020-03550-z
5. He X, Luan F, Yang Y, Wang Z, Zhao Z, Fang J, Wang M, Zuo M, Li Y (2020) *Passiflora edulis*: An insight into current researches on phytochemistry and pharmacology. Front Pharmacol. https://doi.org/10.3389/fphar.2020.00617
6. Yin J, Lin H, Shi J, Lin Z, Bao J, Wang Y, Lin X, Qin Y, Qiu X, Zhang W (2022) Lead-carbon batteries toward future energy storage: from mechanism and materials to applications. Electrochem Energy Rev 5:2. https://doi.org/10.1007/s41918-022-00134-w
7. Aigbe UO, Osibote OA (2024) Green synthesis of metal oxide nanoparticles, and their various applications. J Hazard Mater Adv 13:100401. https://doi.org/10.1016/j.hazadv.2024.100401
8. Khalil AT, Ovais M, Ullah I, Ali M, Jan SA, Shinwari ZK, Maaza M (2020) Bioinspired synthesis of pure massicot phase lead oxide nanoparticles and assessment of their biocompatibility, cytotoxicity and in-vitro biological properties. Arab J Chem 13:916–931. https://doi.org/10.1016/j.arabjc.2017.08.009
9. Abid N, Khan AM, Shujait S, Chaudhary K, Ikram M, Imran M, Haider J, Khan M, Khan Q, Maqbool M (2022) Synthesis of nanomaterials using various top-down and bottom-up approaches. A review, influencing factors, advantages, and disadvantages
10. Omidtorshiz A, Benam MR, Momennezhad M, Sabouri Z, Darroudi M (2023) Green synthesis of lead oxide nanoparticles using *Ocimum basilicum* extract: photocatalytic assessment and cytotoxicity effects. Inorg Chem Commun 158:111575. https://doi.org/10.1016/j.inoche.2023.111575
11. Antolini E (2009) Carbon supports for low-temperature fuel cell catalysts
12. Suffredini HB, Salazar-Banda GR, Avaca LA (2007) Enhanced ethanol oxidation on PbOx-containing electrode materials for fuel cell applications. J Power Sources 171:355–362. https://doi.org/10.1016/j.jpowsour.2007.06.048
13. Bard AJ, Faulkner LR (2001) Electrochemical Methods: Fundamentals and Applications. Wiley, New York
14. Menshykau D, Streeter I, Compton RG (2008) Influence of electrode roughness on cyclic voltammetry. J Phys Chem C 112:14428–14438. https://doi.org/10.1021/jp8047423
15. da Silveira JP, Piovesan JV, Spinelli A (2017) Carbon paste electrode modified with ferrimagnetic nanoparticles for voltammetric detection of the hormone estriol. Microchem J 133:22–30. https://doi.org/10.1016/j.microc.2017.03.010
16. Kinkelin S-J, Röder F, Vogel K, Steimecke M, Bron M (2024) A fundamental study on cyclic voltammetry at porous carbon thin-film electrodes. Electrochim Acta 488:144183. https://doi.org/10.1016/j.electacta.2024.144183
17. Bunge HJ (1997) Influence of texture on powder diffraction. Texture Stress Microstruct 29:1–26. https://doi.org/10.1155/TSM.29.1
18. Li X, Li X, Tang S, Yang J, Li W, Luo B, Yu Y, Li S (2014) High selectivity of benzene electrochemical oxidation to p-benzoquinone on modified PbO2 electrode. Appl Surf Sci 311:357–361. https://doi.org/10.1016/j.apsusc.2014.05.068
19. Cao M, Hu C, Peng G, Qi Y, Wang E (2003) Selected-control synthesis of PbO_2 and Pb_3O_4 single-crystalline nanorods. J Am Chem Soc 125:4982–4983. https://doi.org/10.1021/ja029620l
20. Arami H, Mazloumi M, Khalifehzadeh R, Sadrnezhaad SK (2008) Surfactant free hydrothermal formation of Pb3O4 nanorods. J Alloys Compd 466:323–325. https://doi.org/10.1016/j.jallcom.2007.11.027
21. Cattley CA, Stavrinadis A, Beal R, Moghal J, Cook AG, Grant PS, Smith JM, Assender H, Watt AAR (2010) Colloidal synthesis of lead oxide nanocrystals for photovoltaics. Chem Commun 46:2802. https://doi.org/10.1039/b926176a
22. Gunavathi S, Arulvani K (2024) Eco-Friendly Synthesis of WNPs, PbNPs and AlNPs Nanoparticles Mediated by Waste Peel Extracts of Watermelon (Citrullus Lanatus). Afr J Biomedical Res. https://doi.org/10.53555/AJBR.v27i4S.8166
23. Dongargaonkar AA, Clogston JD (2018) Quantitation of Surface Coating on Nanoparticles Using Thermogravimetric Analysis. Presented at the
24. Martínez-Casado FJ, Ramos-Riesco M, Rodríguez-Cheda JA, Cucinotta F, Matesanz E, Miletto I, Gianotti E, Marchese L, Matěj Z (2016) Unraveling the decomposition process of lead(II) acetate: anhydrous polymorphs, hydrates, and byproducts and room temperature phosphorescence. Inorg Chem 55:8576–8586. https://doi.org/10.1021/acs.inorgchem.6b01116
25. Thakur M, Sharma A, Kumar A, Gautam M, Kumari S (2023) Bio-synthesis of lead oxide nanoparticles using Chinese Mahogany Plant Extract (CMPE@LO) for photocatalytic and antimicrobial activities. Bionanoscience 13:1896–1910. https://doi.org/10.1007/s12668-023-01147-5
26. Czerwiński A, Żelazowska M, Grdeń M, Kuc K, Milewski JD, Nowacki A, Wójcik G, Kopczyk M (2000) Electrochemical behavior of lead in sulfuric acid solutions. J Power Sources 85:49–55. https://doi.org/10.1016/S0378-7753(99)00381-X
27. Heinen M, Jusys Z, Behm RJ (2010) Ethanol, acetaldehyde and acetic acid adsorption/electrooxidation on a Pt thin film electrode under continuous electrolyte flow: an in situ ATR-FTIRS flow cell study. J Phys Chem C 114:9850–9864. https://doi.org/10.1021/jp101441q
28. Wang Y, Wu J, Wang Z, Terenyi A, Giammar DE (2013) Kinetics of lead(IV) oxide (PbO_2) reductive dissolution: role of lead(II) adsorption and surface speciation. J Colloid Interface Sci 389:236–243. https://doi.org/10.1016/j.jcis.2012.09.022
29. Yaqoob L, Noor T, Iqbal N (2021) A comprehensive and critical review of the recent progress in electrocatalysts for the ethanol oxidation reaction. RSC Adv 11:16768–16804. https://doi.org/10.1039/D1RA01841H
30. Zhang X, Wang J, Zong K, Chen Z, Yang X, Yang L, Wang X, Chen Z (2025) Recent advances in non-noble metal-based electrocatalysts for hybrid water electrolysis systems. Carbon Energy. https://doi.org/10.1002/cey2.679
31. Mousavi Z, Benvidi A, Jahanbani S, Mazloum-Ardakani M, Vafazadeh R, Zare HR (2016) Investigation of electrochemical oxidation of methanol at a carbon paste electrode modified with Ni(II)-BS complex and reduced graphene oxide nano sheets. Electroanalysis 28:2985–2992. https://doi.org/10.1002/elan.201501183
32. Barbosa EM, Soares KS, Cruz JF, Doring TH, de França IV, Mello LdosS, Nagurniak GR, Parreira RLT, Alvarenga ME, Martins FT, Dockal ER, Souza EA, Maia PJS, da Cruz JW (2023) Uranyl

N2O2-Schiff base complex as co-catalyst in ethanol electro-oxidation: synthesis, crystallographic, spectroscopic, electrochemical, and DFT characterization, and catalytic investigation. New J Chem 47:17393–17405. https://doi.org/10.1039/d3nj01561k

Publisher's Note Springer Nature remains neutral with regard to jurisdictional claims in published maps and institutional affiliations.